

X-ray magnetic circular dichroism of CeFe₂ by resonant inelastic x-ray scatteringN. Jaouen,¹ S. G. Chiuzbăian,² C. F. Hague,^{1,2} R. Delaunay,² C. Baumier,^{1,2}
J. Lüning,^{1,2} A. Rogalev,³ G. Schmerber,⁴ and J.-P. Kappler⁴¹Synchrotron SOLEIL, L'Orme des Merisiers, Saint-Aubin, Boîte Postale 48, 91192 Gif-sur-Yvette Cedex, France²UPMC Univ. Paris 06, CNRS UMR 7614, Laboratoire de Chimie Physique-Matière et Rayonnement,
75231 Paris Cedex 05, France³ESRF, 6 rue Jules Horowitz, BP 220, 38043 Grenoble Cedex, France⁴IPCMS, UMR 7504, CNRS-UDS, 23 rue de Lœss, BP 43, 67034 Strasbourg Cedex 2, France

(Received 3 March 2010; revised manuscript received 25 April 2010; published 18 May 2010)

We have measured the Ce *L* x-ray magnetic circular dichroism (XMCD) in ferromagnetic CeFe₂ using the partial fluorescence yield given by the Ce *2p3d* resonant inelastic x-ray scattering (RIXS) spectrum. The lifetime broadening of the *3d* core hole is four times smaller than that of the Ce *2p* core hole providing improved resolution over earlier experiments. Clear evidence for a $4f^2$, $4f^1$, $4f^0$ strongly mixed-valent ground state is observed confirming, by and large, impurity Anderson model predictions which take into account the RIXS XMCD geometrical dependence.

DOI: [10.1103/PhysRevB.81.180404](https://doi.org/10.1103/PhysRevB.81.180404)

PACS number(s): 75.30.Mb, 78.20.Ls, 71.20.Eh, 78.70.En

The $4f$ electron configuration in Ce and its intermetallics is known to fluctuate between localized and itinerant-like states leading to a number of unusual properties. First among them is the exceptionally large volume contraction of elemental Ce across the isostructural first order γ - α phase transition which occurs under pressure ($\Delta V/V \approx 15\%$). Configuration fluctuations in the Ce-TM intermetallics (TM stands for a transition metal) also give rise to interesting magnetic properties through hybridization of the Ce *5d* states and *d* states belonging to neighboring TM atoms. In the impurity Anderson model (IAM), the part itinerant, part hybridized nature of the $4f$ states are described formally as a linear combination of $c_n|4f^m v^{2-n}\rangle$ states, where $n=0, 1, \text{ or } 2$; v stands for valence electrons, and c_n is a coefficient.¹ The IAM model is very successful in explaining the observations made by high-energy spectroscopies (see, for example, Refs. 2 and 3). However, much effort has also been put into explaining the ground-state properties by means of *ab initio* local spin-density approximation (LSDA) calculations helped by various techniques to account for correlation and self-interaction effects (see, for instance, Refs. 4 and 5).

CeFe₂, among the Ce intermetallics, has attracted particular attention because it falls into the α -Ce class of materials. It is ferromagnetic with a lower Curie temperature ($T_c=230$ K) and smaller lattice parameter than would be expected by extrapolating from other Laves-phase *R*Fe₂ intermetallics (*R* stands for rare earth).⁶ This explains that x-ray magnetic circular dichroism (XMCD) (Ref. 7) at the Ce *M* (Ref. 8) and Ce *L* (Ref. 9) x-ray absorption edges were among the first such experiments to be performed more than a decade ago.

A closer examination of the Ce *L* XMCD using *2p3d* resonant inelastic x-ray scattering (RIXS) is of interest for several reasons. To start with *2p3d* RIXS at the Ce *L* edge has intrinsically improved resolution compared to x-ray absorption spectroscopy (XAS) measurements because the final state is a Ce *3d* core hole whose lifetime is ≈ 0.7 eV compared to ≈ 3.2 eV for a *2p* core hole. Even though the broadening remains large on the scale of a Kondo resonance, using RIXS provides a unique opportunity to identify contributions

from localized $4f$ electrons highlighted by differences in screening of the final state core hole. Further, it has been shown that it is possible to activate only the absorption followed by emission term of the RIXS XMCD process by choosing suitable geometrical conditions,¹⁰ thus making it directly relevant to the absorption process.

It has also been shown, on the basis of IAM calculations, that RIXS XMCD is sensitive to the ground-state hybridization and the spin-splitting parameters describing the Ce *5d* band.³ Moreover, RIXS at the Ce *L* edge probes the sample to several microns in depth, yet is only weakly subject to self-absorption effects because the *3d-2p* decay channel is not resonant. Other techniques, such as Ce *M* edge XMCD and photoelectron spectroscopies, have the disadvantage of being very surface sensitive.¹¹

Measurements were carried out at the European Synchrotron Radiation Facility beamline ID12.¹² The small incident beam spot size required for optimum resolution with our spectrometer¹³ was obtained by means of a high precision mechanical slit set to 0.05 mm in the vertical plane. The polycrystalline CeFe₂ sample was prepared by arc melting under purified argon atmosphere followed by annealing under high vacuum. It was checked to be single phase by x-ray diffraction. Experiments were performed at a pressure of 10^{-7} mbar. The magnetic field **B** was applied to the sample by means of a permanent magnet placed on a motor-driven rotary platform just below the sample (see Fig. 1) which was cooled to ≈ 20 K. The field of ≈ 0.3 T was sufficient to saturate the magnetic moment.

The *2p3d* RIXS process involving the Ce $2p_{3/2} \rightarrow 5d$ excitation was recorded using a (20 $\bar{2}$ 3) cylindrically bent quartz crystal. The set of RIXS spectra in the scattered photon energy ($\omega_{k'}$) range 4810–4850 eV shown in Fig. 2 were recorded at 90° scattering angle. Data were taken in 0.14 eV steps for a range of incident photon energies (ω_k) from 5710 to 5760 eV. For experimental convenience, XMCD experiments were performed with the spectrometer set to a 45° scattering angle so as to be able to record a nonresonant elastic peak at ≈ 4840 eV to estimate experimental broaden-

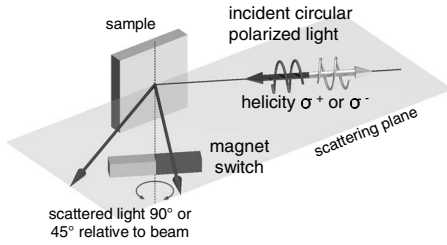


FIG. 1. Schematic of geometrical setup. The angle between the surface of the sample and incoming photon beam was set to 25° . The magnetic field could be rotated to be parallel or antiparallel to the incident photon beam. The scattering angle was either 90° or 45° .

ing. The full width at half maximum of the Gaussian elastic peak was 1.25 eV. The contribution from the ID12 double crystal monochromator is ≈ 0.75 eV, that of the spectrometer is ≈ 1 eV. The $3d$ core-level lifetime broadening is 0.7 eV (Ref. 14) resulting in a total resolution of 1.4 eV.

The magnetic field direction was alternately aligned parallel or antiparallel to the incoming circularly polarized beam with the polycrystalline sample set 25° off-grazing incidence with respect to the beam so no magnetic anisotropy needed to be taken into account as shape anisotropy was minimal. The XMCD data were recorded using the sequence $(\mathbf{B}^+ - \mathbf{B}^-)F^+$, $(\mathbf{B}^- - \mathbf{B}^+)F^-$, $(F^- - F^+)B^+$, see Ref. 7 for definitions.

Figure 2 presents the resonantly excited x-ray emission intensity in the region of the $Ce L\alpha_1(3d_{5/2} - 2p_{3/2})$ and $Ce L\alpha_2(3d_{3/2} - 2p_{3/2})$ decay channels as a function of ω_k across the $Ce L_3$ threshold. The XAS $F^+(\omega_k)$ spectrum measured in the total fluorescence yield (TFY) mode is presented in the top panel of Fig. 3(b) with lower case letters indicating the ω_k values used to record the RIXS spectra. The two *normal* x-ray emission lines lie at 4840.4 eV and 4822.0 eV, respectively.¹⁵ We will consider the higher intensity

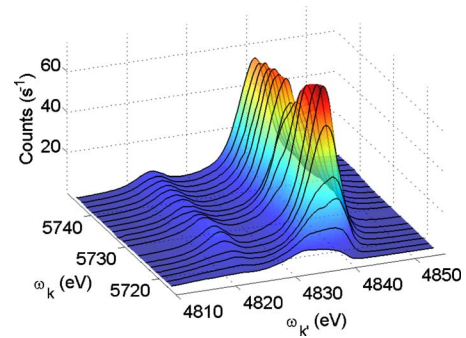


FIG. 2. (Color online) $2p3d$ RIXS data set plotted on a scattered photon energy scale ($\omega_{k'}$) as a function of the incident photon energy (ω_k).

$Ce 3d_{5/2} - 2p_{3/2}$ decay part of the spectrum only. A double structure is apparent in the RIXS data as ω_k starts to increase across the absorption edge. The higher scattered photon energy component increases in intensity as ω_k increases. The scattered photon intensity reaches a maximum at 5727 eV, and then another double structure starts to appear on the low-energy side of the $L\alpha_1$ related peak and, in this case, it is the lower energy component that increases in intensity as ω_k increases. The structures represent typical resonant x-ray Raman processes revealing different final states.

In Fig. 3(a) we plot the RIXS amplitude for two constant values of $\omega_{k'}$ taken from Fig. 2. They relate to the x-ray absorption process measured through two different scattered photon energy windows in the region of the $2p3d$ RIXS. They give access to what is sometimes termed high-resolution XAS though it will be noted that they give a distorted picture of XAS depending on where the cut is made orthogonally to the $\omega_{k'}$ axes. A rigorous use of RIXS for determining the XAS spectrum means recording a complete set of spectra¹⁶ as we have done here. Two sets taken with incident photons of opposite helicity (or reversed magnetiza-

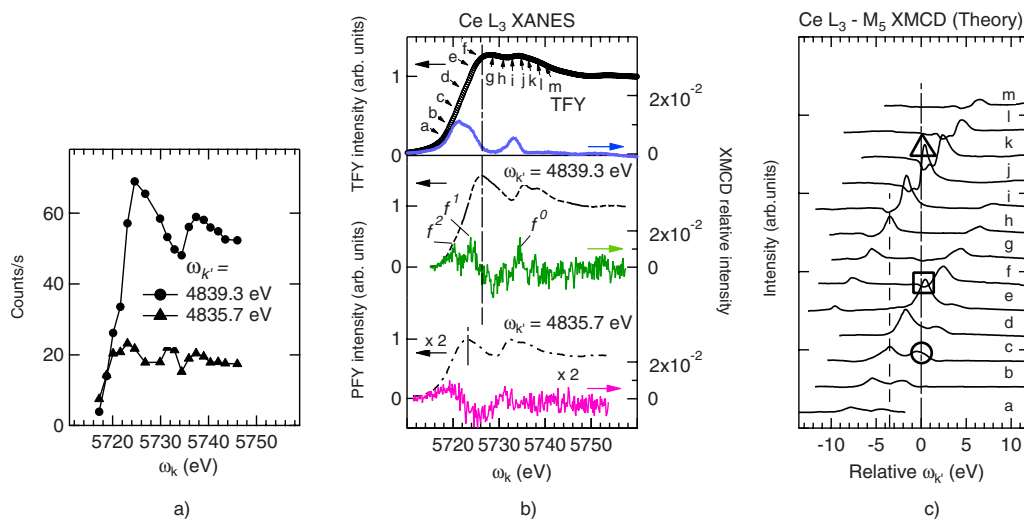


FIG. 3. (Color online) (a) RIXS amplitude at $\omega_{k'} = 4839.3$ and 4835.7 eV as a function of ω_k ; (b) $Ce L_3$ XAS recorded in TFY mode (lower case letters indicate energies used to record RIXS spectra) and XMCD (top panel). PFY spectra taken at $\omega_{k'} = 4839.3$ and 4835.7 eV and XMCD (lower panel); (c) predicted RIXS XMCD adapted from Ref. 19. Symbols are a guide to the ω_k values at which an XMCD resonance is predicted to occur when $\omega_{k'} = 4839.3$ eV.

tion) are needed for XMCD. It is clear that despite a total accumulation time of approximately 48 h for the data set shown in Fig. 2 there is little hope of using this information for measuring an $\approx 1\%$ XMCD signal.

Instead two sets of spectra were taken with the spectrometer set to record the resonant x-ray emission at 4839.3 and 4835.7 eV. The ω_k scans were repeated 10 times. The partial fluorescence yield (PFY) $F^+(\omega_k) + F^-(\omega_k)$ data are presented Fig. 3(b). They correspond to the much coarser data of Fig. 3(a). The XMCD signals $[F^+(\omega_k) - F^-(\omega_k)]$ for the TFY and the PFY curves are also presented in Fig. 3(b).

As a first step toward explaining the Ce L_3 XMCD, Ogasarawa *et al.*,¹⁷ have calculated the Ce $5d$ and Fe $3d$ partial densities of states in the absence of localized $4f$ states using a linear combination of atomic orbitals (LCAO) approach for a Ce₁₇Fe₂₈ cluster. The calculation shows unoccupied hybridized spin-polarized Ce $5d$ and Fe $3d$ states just above E_F and thus a Ce $5d$ related XMCD signal close to E_F where the hybridization occurs between Ce $5d$ and Fe $3d$ states. Otherwise, the Ce $5d$ states form a broad featureless band centered ≈ 4 eV above the Ce L_3 edge once the $2p$ core-hole lifetime and instrumental function have been taken into account. As far as the Fe $3d$ and Ce $5d$ partial DOS are concerned, they agree qualitatively with recent fully relativistic LSDA calculations (Ref. 18) up to about 10 eV above E_F .

The Ce L_3 XAS spectrum deduced from the LCAO calculation is strongly modified, however, when $4f$ hybridization is introduced because of the interaction with the core hole. The main absorption peak in the TFY XAS spectrum is now attributed to the presence of the localized $4f^1$ electron effectively screening the core hole. The dichroism at the onset of the absorption edge continues to reflect the $5d$ polarization but now the poorly screened $4f^0$ part of the spectrum is shifted ≈ 7 eV above the $4f^1$ feature. It explains that there are two relatively narrow XMCD peaks in the TFY experiment.⁹ The XMCD peaks are situated at lower energies with respect to their respective absorption maxima because they result from hybridization with the Fe spin-polarized $3d$ unoccupied states. According to the LSDA calculation,¹⁸ the core-hole interaction can be ignored and the second peak in the XMCD is simply due to spin polarization more than 10 eV above E_F though it is generally recognized that such calculations are somewhat unreliable that far above E_F .

Experimentally, owing to the better performance of the ID12 beamline, structure is visible in the TFY XMCD peak at the onset of the absorption edge [see Fig. 3(b) upper panel] that was not resolved in the early experiments measured by transmission through a powdered sample.⁹ This structure does not have its counterpart in the calculated spectrum based on LSDA-XMCD. We will come back to this later.

The second-order RIXS process can be decomposed into components involving diagonal terms and cross terms.¹⁹ The diagonal terms represent a process where x-ray absorption is followed by x-ray emission and the cross terms involve interference as one goes from the initial to the final state *via* various intermediate states. As mentioned above, Kotani and others have calculated, on the basis of an atomic model, the angular dependence of RIXS XMCD as a function of the

angle between the incident photons and the direction of magnetization (θ_1) and the angle between the direction of magnetization and the observation direction (θ_2). They reveal that for $\theta_1 = 0^\circ$, only the two step component of the second-order optical process contributes to the XMCD. Thus it will depend directly on the first step absorption process. They further show that for $\theta_1 = 0^\circ$ the intensity of the XMCD is practically independent of θ_2 . Thus the TFY measurements using a photodiode in a backscattering geometry should be comparable to our PFY data. Figure 3(c) has been adapted from Ref. 19 to show only the XMCD of a RIXS process at the Ce L_3 edge calculated within the IAM model using a cluster of Ce₃₅Fe₇₆ with $\theta_1 = 0^\circ$ and $\theta_2 = 54.7^\circ$. The calculation was performed for the $2p \rightarrow 5d$ electric dipole (ED) transition: a double peak is seen to disperse at the onset of the absorption (a-e) corresponding to $4f^1$ and $4f^2$ configurations. On an emitted photon energy scale the higher-energy peak belongs to $4f^2$. As ω_k reaches the region e-m another peak followed by a dip disperses across the constant ω_k' line and this is attributed to the $4f^0$ part of the spectrum.

The XMCD signals obtained from the RIXS experiments tend to confirm the IAM theoretical predictions, though some important discrepancies are also evident. First the relative intensities of the $4f^1$ and $4f^2$ related peaks in the RIXS XMCD are not reproduced by the theory. The TFY XMCD shown in the top panel of Fig. 3(b) also suggests that the lower-energy peak is more intense than that at higher energy. In the PFY spectrum taken at $\omega_k' = 4839.3$ eV all three peaks are narrow and have approximately the same amplitude. The PFY spectrum at $\omega_k' = 4835.7$ eV has shifted to lower ω_k' by 3.6 eV which is to be expected. An equivalent shift in ω_k' is marked by a dashed line in Fig. 3(c) which illustrates how the $4f^2$ structure will resonate at a lower value of ω_k , albeit more weakly, and explains that the $4f^1$ and $4f^2$ peaks are not resolved. The broad dip ≈ 4.6 eV above the $4f^1$ peak is confirmed. This dip is absent both from the IAM theory and the TFY XMCD data. On the other hand, we note that the LSDA-XMCD features a dip ≈ 5 eV above E_F . If we assume that the dipole excitation probes the unoccupied Ce $5d$ states simply offset by the effect of $4f$ screening of the final state core hole, this could be a feature of the ground-state spin density of states. Its absence from the TFY XMCD might be attributed to the intrinsically poorer resolving power. The valley between the $4f^1$ and $4f^0$ peaks is shallower still in the XMCD originally measured in the transmission mode.⁹

The contribution from the $2p \rightarrow 4f$ electric quadrupole (EQ) transition is not included in the theory. Here again Kotani and others have investigated the angular dependence of EQ transitions and found that when $\theta_1 = 0^\circ$ the cross term is zero²⁰ so that, similarly to ED, the EQ channel can be considered to contribute quite straightforwardly to the XMCD signal *via* an absorption followed by emission process. In a purely ionic Ce compound it has been demonstrated experimentally that the $2p^5 \rightarrow 4f^{n+1}$ EQ contribution is $\approx 2\%$ of the ED RIXS intensity.²¹ For the EQ process to have sufficient impact on the intensity of the $4f^2$ XMCD, the ground state $4f^1$ -related state would have to be very strongly magnetically spin polarized since the XMCD itself is only about $\approx 2\%$ of the XAS intensity. This is specifically assumed not to be the case in the model used to perform the RIXS XMCD calculations.¹⁹

The consensus has long been that the $4f$ states in CeFe_2 form a broad itinerant band quite well described by LSDA (see, for instance, Ref. 18). This has been challenged recently both on the grounds that the $4f$ orbital contribution to the magnetic moment is not negligible (see Ref. 22) and because bulk-sensitive resonant photoemission at the Ce M_5 edge point to localized states in α -like Ce intermetallics.²³ Our observation makes a major contribution to the mounting

evidence of a strongly mixed-valent system for CeFe_2 even if a quantitative assessment must await a better understanding of the relative weights of the ED and EQ processes in the resonant inelastically scattered XMCD signal.

We acknowledge the European Synchrotron Radiation Facility and are particularly indebted to S. Feite and M. Perez for assistance in interfacing with ID12 beamline devices.

-
- ¹O. Gunnarsson, K. Schönhammer, J. C. Fuggle, F. U. Hillebrecht, J.-M. Esteve, R. C. Karnatak, and B. Hillebrand, *Phys. Rev. B* **28**, 7330 (1983).
- ²A. Kotani, *Eur. Phys. J. B* **47**, 3 (2005).
- ³A. Kotani, *Phys. Rev. B* **78**, 195115 (2008).
- ⁴Z. Szotek, W. M. Temmerman, and H. Winter, *Phys. Rev. Lett.* **72**, 1244 (1994).
- ⁵A. K. McMahan, K. Held, and R. T. Scalettar, *Phys. Rev. B* **67**, 075108 (2003).
- ⁶O. Eriksson, L. Nordström, M. S. S. Brooks, and B. Johansson, *Phys. Rev. Lett.* **60**, 2523 (1988).
- ⁷The XMCD signal is the difference in intensity between $F^+(\omega)$ and $F^-(\omega)$, where F^+ (F^-) represents a clockwise (anticlockwise) circularly polarized beam traveling toward an antiparallel magnetic field \mathbf{B} and ω is the photon energy.
- ⁸A. Delobbe, A.-M. Dias, M. Finazzi, L. Stichauer, J.-P. Kappler, and G. Krill, *Europhys. Lett.* **43**, 320 (1998).
- ⁹C. Giorgetti *et al.*, *Phys. Rev. B* **48**, 12732 (1993).
- ¹⁰K. Fukui, H. Ogasawara, A. Kotani, T. Iwazumi, H. Shoji, and T. Nakamura, *J. Phys. Soc. Jpn.* **70**, 3457 (2001).
- ¹¹E. Cho *et al.*, *Phys. Rev. B* **67**, 155107 (2003).
- ¹²J. Goulon, N. B. Brookes, C. Gauthier, J. Goedkoop, C. Goulon-Ginet, M. Hagelstein, and A. Rogalev, *Physica B* **208-209**, 199 (1995).
- ¹³C. F. Hague, J.-M. Mariot, L. Journel, J.-J. Gallet, A. Rogalev, G. Krill, and J.-P. Kappler, *J. Electron Spectrosc. Relat. Phenom.* **110-111**, 179 (2000).
- ¹⁴J. L. Campbell and T. Papp, *At. Data Nucl. Data Tables* **77**, 1 (2001).
- ¹⁵J. A. Bearden, *Rev. Mod. Phys.* **39**, 78 (1967).
- ¹⁶P. Carra, M. Fabrizio, and B. T. Thole, *Phys. Rev. Lett.* **74**, 3700 (1995).
- ¹⁷H. Ogasawara, K. Asakura, K. Fukui, I. Harada, and A. Kotani, *J. Phys. Chem. Solids* **63**, 1485 (2002).
- ¹⁸V. N. Antonov, D. A. Kukusta, and A. N. Yaresko, *Phys. Rev. B* **78**, 094401 (2008).
- ¹⁹K. Asakura, A. Kotani, and I. Harada, *J. Phys. Soc. Jpn.* **74**, 1328 (2005).
- ²⁰K. Fukui and A. Kotani, *J. Phys. Soc. Jpn.* **73**, 1059 (2004).
- ²¹L. Journel *et al.*, *Phys. Rev. B* **66**, 045106 (2002).
- ²²M. S. S. Brooks, *Physica B* **345**, 93 (2004).
- ²³R.-J. Jung, B.-H. Choi, S.-J. Oh, H.-D. Kim, E.-J. Cho, T. Iwasaki, A. Sekiyama, S. Imada, S. Suga, and J.-G. Park, *Phys. Rev. Lett.* **91**, 157601 (2003).